Appl. Phys. A (2016)122:102
DOI 10.1007/s00339-016-9638-1

Applied Physics A
Materials Science & Processing

Effect of cerium doping on the structural, morphological, photoluminescent and thermoluminescent properties of sodium strontium pentaborate microstructures

S. W. Joo[1] · B. Deva Prasad Raju[2] · G. R. Dillip[1] · A. N. Banerjee[1] · J. H. Jung[3]

Received: 12 September 2015 / Accepted: 15 January 2016

Abstract We have reported a new blue-emitting cerium (Ce^{3+})-doped sodium strontium pentaborate ($Na_3SrB_5O_{10}$) microstructures via a conventional high-temperature solid-state reaction route. X-ray diffraction analysis revealed the phosphors crystallized in triclinic structure. Significantly, well-shaped morphology in micrometer dimension phosphors was identified by field emission scanning electron microscopy. The phosphors displayed a single broad blue emission centered at around 370 nm because of the Ce^{3+} 5*d*–4*f* transition under the excitation wavelength of 232 nm. In the region of room temperature to 350 °C, the thermoluminescence (TL) glow curves consist of only one sharp peak located at about 200.31 °C. The optimum concentration of Ce^{3+} for TL and PL intensity was found to be 1 at.% in host. These results suggest that the newly proposed $Na_3SrB_5O_{10}$:Ce^{3+} phosphor with the suitable TL emission ($T_m \sim 200$ °C) in micrometer dimension might potentially be used for thermoluminescence dosimetric applications.

S. W. Joo and B. Deva Prasad Raju have contributed equally to this work.

✉ G. R. Dillip
dillip.ngr@gmail.com

✉ A. N. Banerjee
arghya@ynu.ac.kr; banerjee_arghya@hotmail.com

✉ J. H. Jung
jhjung@ynu.ac.kr

[1] School of Mechanical Engineering and Technology, Yeungnam University, Gyeongsan 712 749, South Korea

[2] Department of Future Studies, Sri Venkateswara University, Tirupati 517 502, India

[3] School of Chemical Engineering, Yeungnam University, Gyeongsan 712 749, South Korea

1 Introduction

Over the recent past, due to increased interest of the researchers, they have been devoted to studying the borate materials for thermoluminescence dosimetric (TLD) applications because of their rich variety in structure, wide transmittance spectra with high damage threshold, good chemical and physical stability and wide band gaps [1–3]. Although various materials as TL materials have been used in several applications, many efforts are placed on better tissue equivalence, neutron and gamma sensitive to develop new TL materials. Particularly, the TL materials based on borates have been considered as one of the most promising materials in dosimetry due to their tissue-equivalent absorption coefficient and neutron sensitivity [4, 5]. Currently, there is a great demand of the dosimetric phosphors, which exhibit simple and sharp glow curves. In the literature, a large number of TL materials have been investigated [6–9]; among them not all of the materials to be attractive for dosimetry, especially for application in connection with personal and environmental dosimetry. But, the obtained results provide the useful information regarding the defect and trap structure that will result in search for new borate TLD material for further research in this field. Therefore, efforts are being made either to develop novel phosphors or to improve the existing ones. The researchers in the field of luminescence have special interest in Ce^{3+}-doped materials because of their low cost, spin and parity allowed optical 4*f*–5*d* transitions and have a fast radiative lifetime of about 10–50 ns. It is desirable for applications in scintillators, light-emitting diodes (LEDs) and field emission displays (FEDs). And also covalence allows altering the energy difference between 4*f* and 5*d* levels of Ce^{3+} ions in the crystal lattice, which alters the emission at different wavelengths [10–13]. Over the past

Published online: 28 January 2016

few decades, extensive research has been carried out on Ce^{3+}-doped borates because of their enormous applications in phosphors, UV-absorbing filters (or) UV emitters and activators for energy transfer, detectors for ionizing radiation, scintillators for elemental particles, imaging, lithography, optical data recording, solid-state lasers and displays [14–16]. Generally, the Ce^{3+} is optically active, and the emission occurs typically in UV/blue region depending upon the host structure and 4*f*–5*d* transition. Ce^{3+} ion plays an important role as an activator in the TL phosphors and its emission, intense enough to be used for practical applications. It is known that usually the Ce^{3+} emission results from 5*d* to 4*f* type of transition while the *f*–*f* transition occurs in the IR region. The ground state of Ce^{3+} splits into $^2F_{5/2}$ and $^2F_{7/2}$ levels for possible 4*f* configuration. The emission results above the $^2F_{7/2}$ excited state correspond to 5*d* configuration in the form of broad bands [17, 18].

Recently, Wu et al. [19] reported the synthesis of a new borate, $Na_3SrB_5O_{10}$, crystallized in triclinic structure. In the previous paper, our group studied and explored systematically, the Dy^{3+}-doped $Na_3SrB_5O_{10}$ phosphors for solid-state lighting [20] application. In the present work, the photoluminescence and thermoluminescence properties of Ce^{3+}-doped $Na_3SrB_5O_{10}$ material were investigated. To the best of our knowledge, no reports have appeared in the literature on optical and thermal properties of Ce^{3+}-doped $Na_3SrB_5O_{10}$ host. For the first time, the trapping parameters such as order of kinetics (*b*), activation energy (*E*) and frequency factor (*s*) of $Na_3SrB_5O_{10}$:Ce^{3+} phosphors were estimated using Chen's full width method, and the obtained results were discussed and reported in detail. The TL dosimetric properties of Ce^{3+}-doped $Na_3SrB_5O_{10}$ microstructures were examined under the irradiation of γ-rays, indicating that the proposed phosphors might be a potential material for radiation dosimetry.

2 Experimental

In general, synthesis of borate compounds is quite difficult because of the fact that it may form crystalline as well as glassy phase based on the method of selection. For obtaining efficient luminescent materials, the crystalline form is essential. In the present study, to receive pure phase of the final product, the Ce^{3+}-doped $Na_3SrB_5O_{10}$ polycrystalline phosphors were synthesized by a single-step solid-state reaction method. The starting materials were of high-purity (99.9 %) analytical reagent (AR) grade of Na_2CO_3, $SrCO_3$, H_3BO_3 and CeO_2 used as received without further purification. The concentration of Ce^{3+} was fixed at 0.5, 1, 3 and 5 at.% in the host matrix. In the first step, the stoichiometric amounts of raw materials were mixed and ground homogenously in an agate mortar for 1 h. Then, the mixture was transferred into a porcelain crucible and calcined in an electric furnace at 800 °C for 8 h. After that, the samples were furnace-cooled to room temperature (RT) and finally ground again into powder for further measurements.

Structure of the as-prepared phosphors was analyzed using a PANalytical X'pert PRO X-ray diffractometer with CuK_α radiation ($\lambda = 0.154056$ nm) at 40 kV and 30 mA. The data were recorded over a 2θ range from 20° to 80° in the step-scan mode with a step size of 0.02°. Fourier transform infrared (FTIR) spectra were measured on a Bruker Alpha-T FTIR spectrophotometer using KBr pellets in the spectral range between 4000 and 500 cm^{-1}. The microstructure of samples was investigated using a field emission scanning electron microscope (FE-SEM, Hitachi S-4200, Japan), and elemental analysis was carried out by energy-dispersive X-ray analysis (EDS) on the FE-SEM attached X-ray column. To improve the conductivity of the samples, an ultra-thin layer of platinum was sputter-coated (E-1030 Ion sputter, Hitachi, Japan) on the sample surface. UV–Vis diffuse reflectance spectra (DRS) were measured on a UV–Vis–NIR spectrophotometer (Jobin Varian Cary 5000, USA) using a polytetrafluoroethylene (PTFE) as a standard. Photoluminescence excitation (PLE) and emission (PL) properties were characterized on a Jobin–Yvon Fluorolog-3 Fluorimeter with a 150-W Xe lamp as the excitation source. All the measurements were taken at RT. For thermoluminescence studies, the powders were exposed to gamma (γ) rays from a ^{60}Co source at a rate of 0.58 $kGyh^{-1}$ for 5 Gy. TL glow curves were recorded at two different irradiation times of 30 s and 5 min. In order to reduce the error, after the desired exposure time, at the same dose, the glow curves were measured immediately on a standard TL reader Harshaw-3500 between RT and 350 °C at a heating rate of 5 °C/s.

3 Results and discussion

3.1 XRD studies

XRD patterns of the $Na_3SrB_5O_{10}$:Ce^{3+} phosphors (Ce^{3+} = 0.5, 1, 3 and 5 at.%) are shown in Fig. 1. For all samples, the dominant diffraction peaks were well indexed as the $Na_3SrB_5O_{10}$ borate crystal of triclinic structure reported by the Crystallography Open Database (COD) ID no: 2016662. Due to the increase in CeO_2 concentration in the host, the predominant diffraction peaks are shifted toward higher 2θ angle side, suggesting that the introduced Ce^{3+} ions might be substituted in the host cation sites. According to ionic radii of Na^+ (1.02 Å, coordination number (CN) = 6)/Sr^{2+} (1.26 Å, CN = 8)/B^{3+} (0.11 Å,

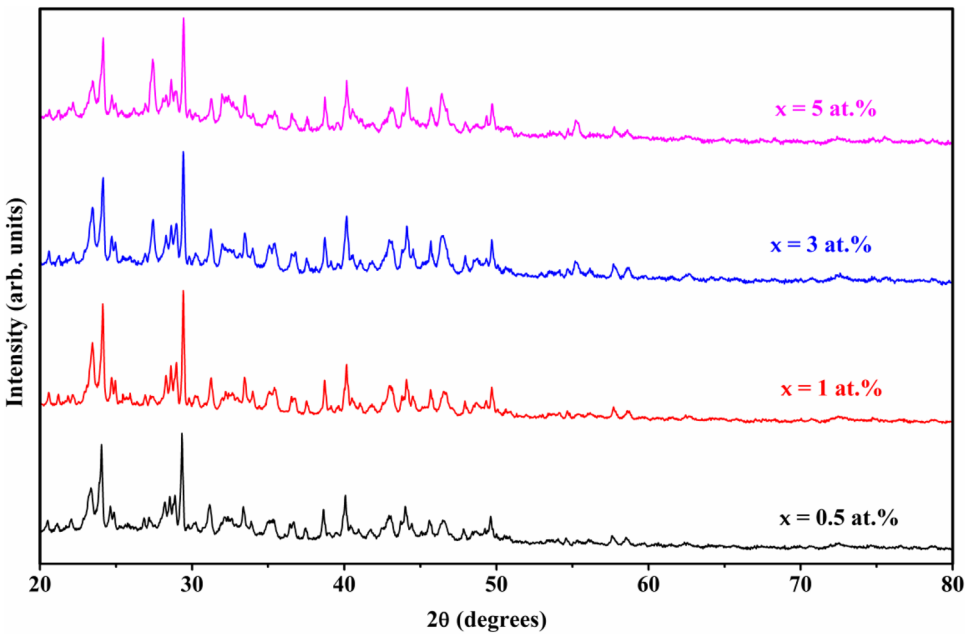

Fig. 1 XRD patterns of $Na_3Sr_{1-x}B_5O_{10}:Ce_x^{3+}$ phosphors ($x = 0.5 - 5$ at.%)

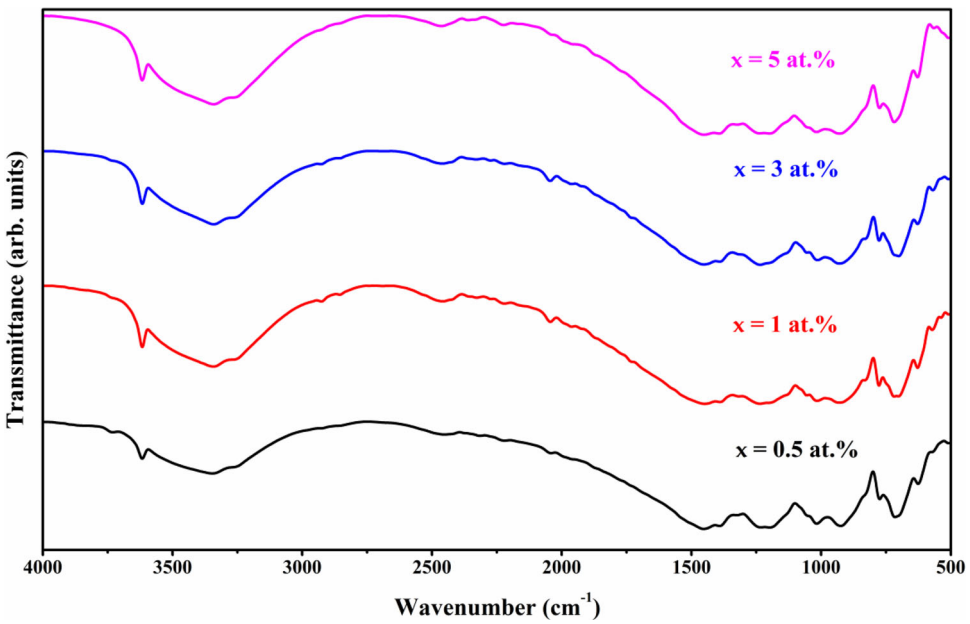

Fig. 2 FTIR spectra of $Na_3Sr_{1-x}B_5O_{10}:Ce_x^{3+}$ phosphors ($x = 0.5 - 5$ at.%)

CN = 4)/Ce^{3+} (1.14 Å, CN = 8) and disparity of ionic states, the Ce^{3+} ions would preferably occupy at the Na^+/Sr^{2+} cation sites in $Na_3SrB_5O_{10}$ crystal [21, 22]. This is because of the similar ionic radii of both the ions (Na^+ and Sr^{2+}). In general, when a metal cation is substituted for an ion with a different valence in the host lattice like $Na_3SrB_5O_{10}$, the charge compensator, such as, Na^+ is employed to keep the charge balance. Therefore, the charge compensation in the $Na_3SrB_5O_{10}:Ce^{3+}$ phosphor is most likely to be described by two possible mechanisms:

1. Two Sr^{2+} ions are replaced by one Ce^{3+} ion and one alkaline cation,

$$2Sr^{2+} \rightarrow Ce^{3+}M^{+};\ M^{+}\text{is an alkaline cation like } Na^{+} \quad (1)$$

2. Charge compensation by a strontium vacancy,

$$3Sr^{2+} \rightarrow 2Ce^{3+} + V_{Sr} \quad (2)$$

3.2 FTIR studies

In order to confirm the coordination surrounding the B–O in $Na_3SrB_5O_{10}:Ce^{3+}$ phosphors, the FTIR spectra were recorded and are described in Fig. 2. We note from the figure that the assignment of vibrations for all samples was similar in nature and no significant peak shifting was observed. The bands observed in the region of 1460 to 1225 cm^{-1} correspond to the BO_3 asymmetric stretching vibrations, while the bands between 1055 and 925 cm^{-1} are due to the BO_4 asymmetric stretching modes. The bands associated with BO_3 and BO_4 out-of-plane bending modes are overlapped and located in the range of 820 to 705 cm^{-1}. The vibrations below 550 cm^{-1} should be ascribed to the Na–O and Sr–O vibrations [23]. The broad absorption band with a sharp shoulder at about 3340 and 3617 cm^{-1}, respectively, suggests the presence of –OH group in the samples [24]. These vibrations usually arise from physically absorbed water molecules on the samples surface during the grinding process to make the KBr pellet under non-vacuum condition.

3.3 FE-SEM and EDS studies

Figure 3 shows the surface morphology of Ce^{3+}-doped $Na_3SrB_5O_{10}$ powders. In the figure, the morphology of samples is similar to appear, even though a slight aggregation of particles was seen in the figure that usually occurs during the high calcination. However, the agglomeration is decreased due to the increase in Ce^{3+} ions content in the host, suggesting the solubility of dopant in $Na_3SrB_5O_{10}$ crystal. A closer look at the micrograms clearly suggests that the morphology of the synthesized phosphors appears to have hexagonal plate-like morphology (*highlighted in the images by white circles*). Therefore, this kind of defined morphology of phosphor might be act as a potential candidate in luminescence applications. To identify the presence of elements in the $Na_3SrB_5O_{10}:Ce^{3+}$ phosphors, qualitatively the EDS analysis was carried out. Figure 4 shows the EDS spectra of Ce-doped $Na_3SrB_5O_{10}$ microstructures. It confirmed the presence of Ce element in the $Na_3SrB_5O_{10}:Ce^{3+}$ phosphors. For reference, the authors presented a table (inset of Fig. 4c), which represents the qualitative estimation of elemental percentage of Na, Sr, O and Ce. The elemental peaks of C and Pt are appeared in spectra due to the carbon tap and coated platinum particles on the sample surface, respectively. Hence, the absence of other impurity elements in EDS profiles is an evidence of the purity of prepared sample, which are matched well with the structural analysis.

3.4 DRS studies

DRS of the $Na_3SrB_5O_{10}:Ce^{3+}$ (Ce^{3+} = 0.5, 1, 3 and 5 at.%) phosphors are depicted in Fig. 5a. In the range of 800 to 400 nm, all the samples show platform of high reflectance and then start to decrease between 400 and 200 nm. In the range of 400 to 200 nm, a couple of absorption bands at around 231 and 270 nm correspond to the $4f$–$5d$ transition of Ce^{3+} ion [25]. The similar bands are also observed in the excitation spectrum. Therefore, due to the increase in dopant concentration in the host material, the enhancement of optical absorption in UV region was observed.

3.5 Photoluminescence properties

The photoluminescence excitation spectrum of the $Na_3SrB_5O_{10}:Ce^{3+}$ (Ce^{3+} = 1 at.%) phosphor monitored at 370 nm emission is shown in inset of Fig. 5b. The spectrum composed of five bands, located at around 232, 259, 305, 323 and 332 nm that are corresponding to the transitions from the Ce^{3+} $4f^1$ ($^2F_{5/2}$) ground state to the various $4f^0$ ($5d^1$) crystal-field components. These bands show that the crystal-field splitting of Ce^{3+} $5d$ level completely split into five levels $5d(1)$, $5d(2)$, $5d(3)$, $5d(4)$ and $5d(5)$ at about 5.34, 4.79, 4.06, 3.84 and 3.73 eV energies, respectively [26]. Among the absorption bands, we used the excitation wavelength of 232 nm to further record the emission spectra of phosphors. Figure 5b describes the emission spectra of $Na_3SrB_5O_{10}:Ce^{3+}$ phosphors as a function of Ce^{3+} ions. The spectra consist of only single broad band in the range from 350 to 450 nm, for all the samples with similar profiles peaked at around 370 nm. In the literature, many reports have appeared on the similar emission bands [14, 27–29]. For instance, Nagaoka and Adachi [28] reported the emission spectra of $NaCl:Ce^{3+}$ phosphor, peaked at 360 nm (blue emission) under the excitation of 269 nm. Kore et al. [29] explored the photoluminescence properties of $Na_6Mg(SO_4)_4$:RE (RE = Ce, Tb) phosphors, and they obtained single broad emission band centered at 355 nm (λ_{ex} = 300 nm). In our present investigation, the authors obtained a single broad emission band peaked at 370 nm under the excitation wavelength of 232 nm at RT. This broad band is ascribed to the excited state $5d$ to $4f$ ground state transition of Ce^{3+} ions. However, due to the increase in Ce^{3+} ions concentration, the emission intensity also increased and reached maximum at 1 at.%, and then, the intensity declined drastically for 3 and 5 at.% of Ce^{3+} ions, respectively. This is due to the concentration quenching. According to Dexter's theory [30], the concentration quenching occurs by the non-radiative energy migration between identical activators inside the host crystal. Furthermore, to find electric multipolar interaction

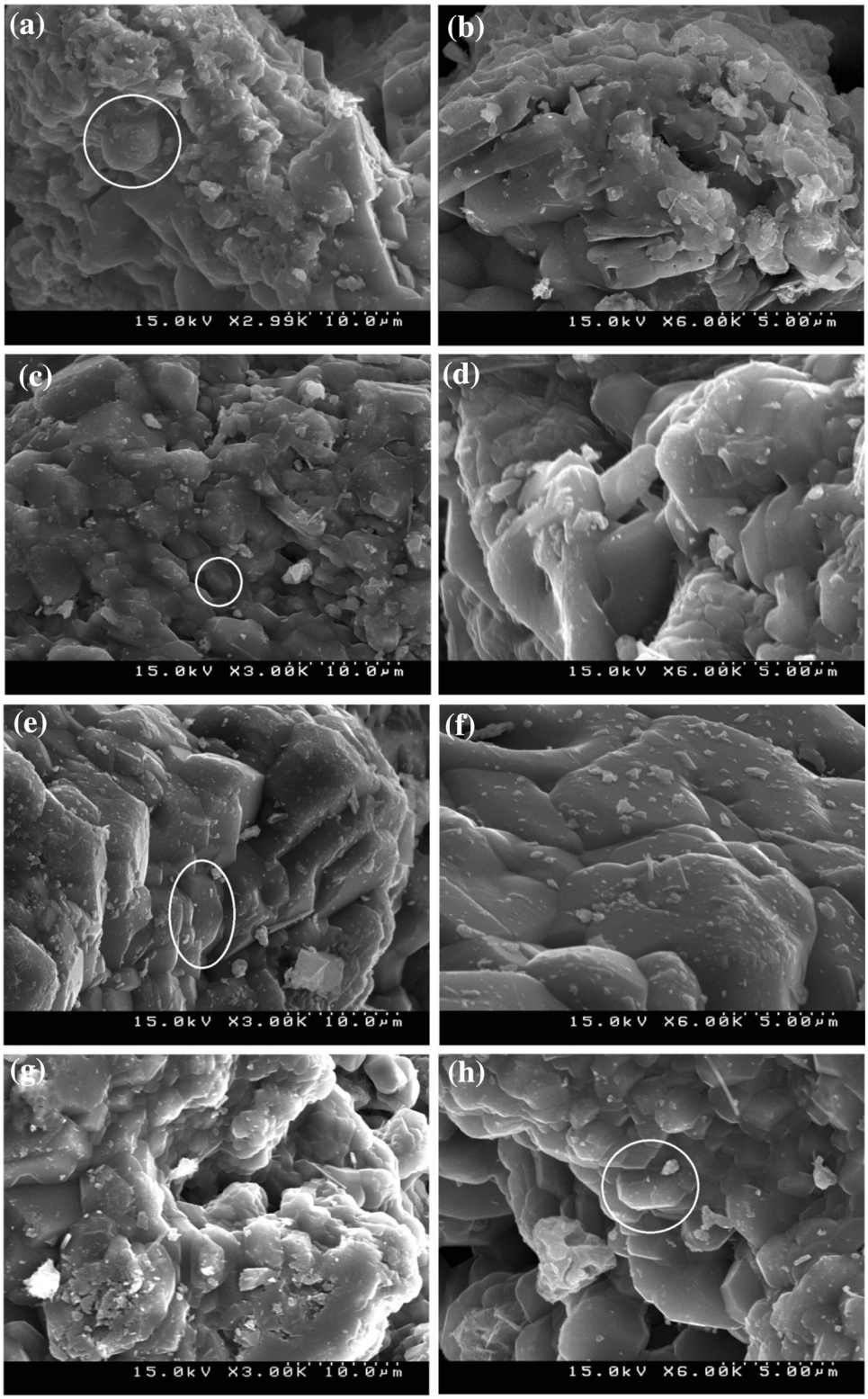

Fig. 3 SEM images of $Na_3Sr_{1-x}B_5O_{10}:Ce_x^{3+}$ phosphors ($x = 0.5 - 5$ at.%); **a**, **b** $x = 0.5$ at.%, **c**, **d** $x = 1$ at.%, **e**, **f** $x = 3$ at.% and **g**, **h** $x = 5$ at.%

mechanism in Ce^{3+}-doped $Na_3SrB_5O_{10}$ phosphor, the emission intensity (I) per activator ion was calculated according to the Van Uitert equation [31];

$$\frac{I}{x} = k\left[1 + \beta(x)^{\theta/d}\right]^{-1} \quad (3)$$

where I/x is the emission intensity per activator content,

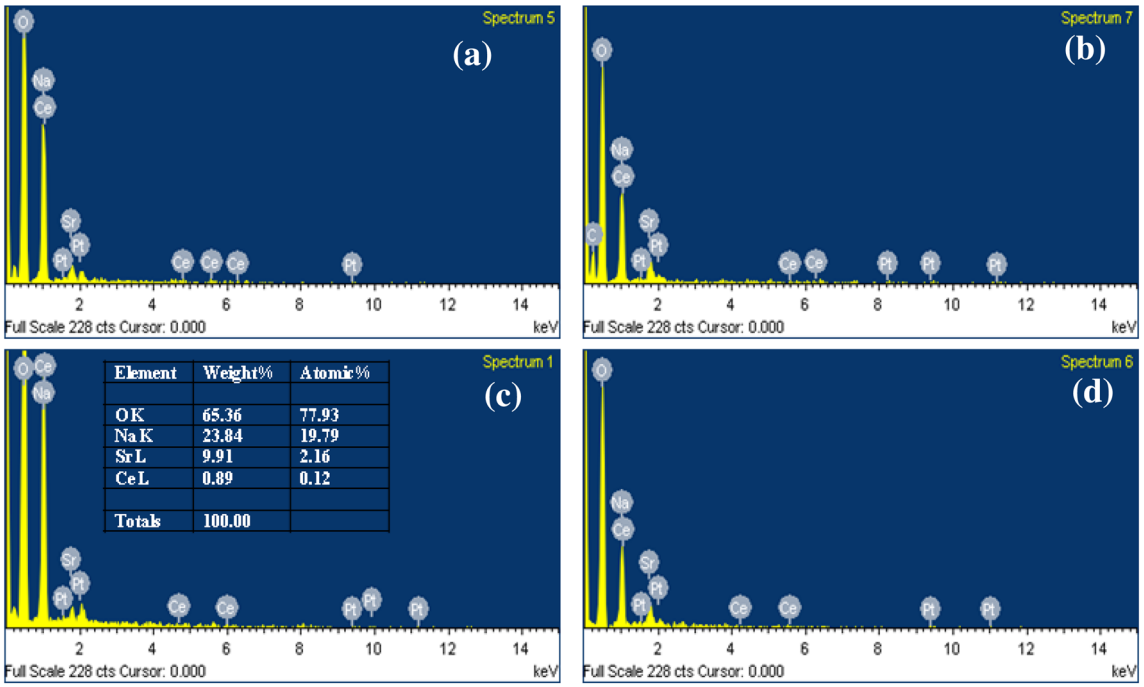

Fig. 4 EDS profiles of $Na_3Sr_{1-x}B_5O_{10}:Ce_x^{3+}$ phosphors ($x = 0.5 - 5$ at.%); **a** $x = 0.5$ at.%, **b** $x = 1$ at.%, **c** $x = 3$ at.% and **d** $x = 5$ at.%. *Inset* of **c** shows the elemental percentage of $Na_3Sr_{1-x}B_5O_{10}:Ce_x^{3+}$ phosphor ($x = 3$ at.%)

x is the activator concentration, which is not less than the critical concentration, d is the sample dimension ($d = 3$ for energy transfer among the activators inside particles), k and β are the constants (independent of activator concentration), and θ is an indication of electric multipolar. The index θ could be 6, 8 and 10 for the dipole–dipole (d–d), dipole–quadrupole (d–q) and quadrupole–quadrupole (q–q) electric interactions, respectively, and $\theta = 3$ corresponds to exchange interactions. To find value of θ, the log (I/x) dependence of log (x) at 370 nm emission is plotted and is shown in Fig. 5c, which gives a linear fit having an y-intercept, 1.6448 and a slope ($-\theta/3$) of -1.0287. The value of θ estimated to be ~ 3.08, which is close to 3. Hence, the concentration quenching for the two Ce^{3+} ions results from exchange interaction in the $Na_3SrB_5O_{10}:Ce^{3+}$ phosphors. It is known that the distance between identical activators could be found by critical distance (R_c) using the following formula [32],

$$R_C \approx 2\left[\frac{3V}{4\pi x_c N}\right]^{1/3} \quad (4)$$

where V is the volume of unit cell (Å^3), X_c is the critical concentration of activator ions (at.%), and N is the number of host cations (Sr^{2+}) in the unit cell. In the present phosphor, the values of V, X_c, and N are considered to be 446.47 Å^3, 0.01 and 2, respectively [19]. The value of R_c is found to be around 34.09 Å. Moreover, to examine the emission color of phosphor, the International Commission on Illumination (CIE) 1931 chromatic coordinates are calculated. The estimated chromaticity coordinates of $Na_3SrB_5O_{10}:Ce^{3+}$ phosphor ($Ce^{3+} = 1$ at.%) are located in blue region, as shown in CIE diagram in Fig. 5d.

3.6 Thermoluminescence properties

To examine the defect properties of Ce^{3+}-doped $Na_3SrB_5O_{10}$ phosphors, the thermoluminescence studies were carried out. In general, the analysis of TL spectrum provides useful information of the presence of trapping centers and their distribution in the borate materials. Figure 6a, b shows the typical TL glow curves of $Na_3SrB_5O_{10}:Ce^{3+}$ microstructures, irradiated at a dose of 0.58 KGyh^{-1} for 5 Gy with irradiation times of 30 s and 5 min, respectively. The glow curves consist of a single broad band having similar profiles for various concentrations of the Ce^{3+} ions, measured in both the exposure times (5 and 30 min). However, various peak positions and intensities are observed for different concentrations of Ce^{3+}. It is known that a simple glow curve with a high-temperature TL glow peak around 200 °C shows the high-temperature traps that are formed during gamma ray irradiation, and these are not decay at RT [5]. Hence, it is a key characteristic of the TLD material. In our present investigation, we obtained a simple glow curve with a main peak at about 200.31 °C for 1 at.% Ce^{3+}-doped $Na_3SrB_5O_{10}$ phosphor at 5 min of γ-ray irradiation. For lower concentration of Ce^{3+} ions, the shape

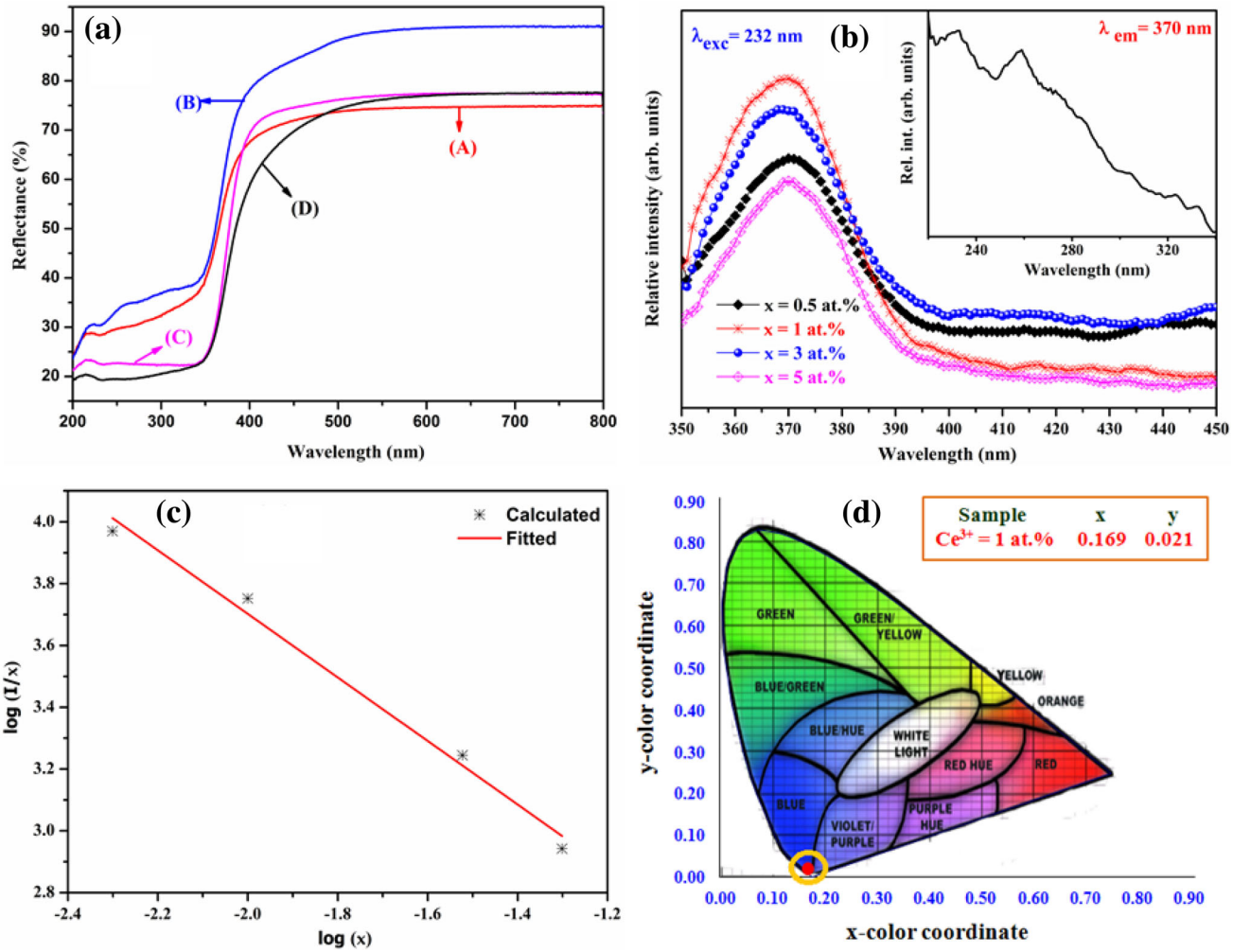

Fig. 5 **a** UV–Vis DRS of $Na_3Sr_{1-x}B_5O_{10}:Ce_x^{3+}$ phosphors (x = A–D = 0.5 − 5 at.%), **b** emission spectra of $Na_3Sr_{1-x}B_5O_{10}:Ce_x^{3+}$ phosphors (x = 0.5 – 5 at.%) and *inset* shows the excitation spectrum of $Na_3Sr_{1-x}B_5O_{10}:Ce_x^{3+}$ phosphor (x = 1 at.%), **c** plot of log (I/x) versus log (x) and **d** CIE chromaticity coordinates of $Na_3Sr_{1-x}B_5O_{10}:Ce_x^{3+}$ phosphor (x = 1 at.%)

of the glow curve is dissymmetrical and the area of the low-temperature side is obviously larger than that of the high-temperature side. However, the symmetrical nature of the curves is varying according to the Ce^{3+} concentration, as shown in Fig. 6c–f for reference. Due to the increase in Ce concentration, the TL intensity also increased up to 1 at.%, and then, the intensity decreased with further increase in dopant concentration in both the exposure times. It is owing to concentration quenching of dopant element. Therefore, the optimum Ce^{3+} concentration is found to be 1 at.% in $Na_3SrB_5O_{10}$. In addition, the parameters such as order of kinetics (b), activation energy (E) and frequency factor (s) correspond to the TL peaks can be obtained by analyzing the glow curves using Chen's peak shape method [33]. By using this method, one can overcome the geometrical reproducibility and problem of contact of a sample with the heating planchet that apparently alter the kinetics. According to Chen's full width method, the geometrical factor μ_g of a TL peak is determined by the following equation,

$$\mu_g = \frac{\delta}{\varepsilon} = \frac{(T_2 - T_m)}{(T_2 - T_1)} \tag{5}$$

where T_1, T_2 and T_m are the temperature of half intensity on the low- and high-temperature side, and the peak temperature of the TL peak, respectively. The value of μ_g is 0.42 and 0.52 for first- and second-order kinetics, respectively. The estimated values are presented in Table 1. The geometrical factor values are varying from first-order kinetics to second-order kinetics due to the increase in Ce^{3+} concentration. Furthermore, to support these results, the order of kinetics is also estimated according to Balarin parameter and is given by the following equation [34];

$$\gamma = \frac{\delta}{\tau} = \frac{(T_2 - T_m)}{(T_m - T_1)} \tag{6}$$

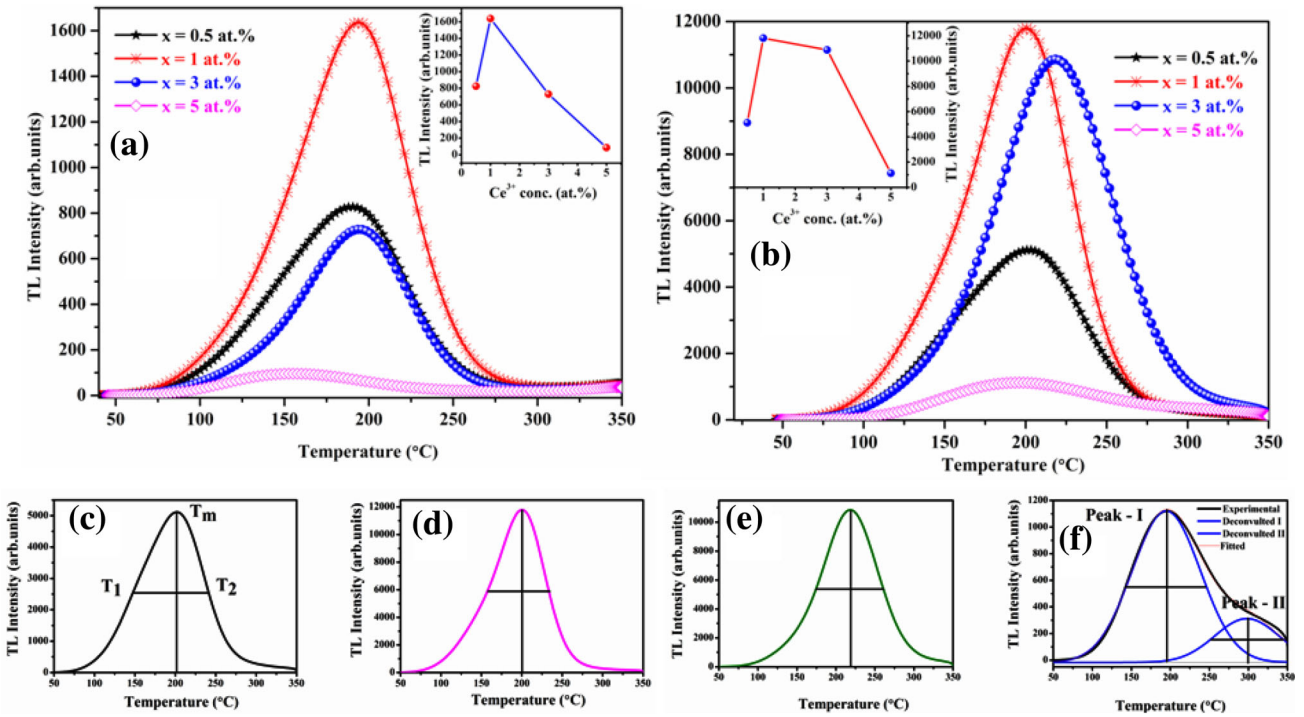

Fig. 6 Thermoluminescence glow curves of $Na_3Sr_{1-x}B_5O_{10}:Ce_x^{3+}$ phosphors ($x = 0.5 - 5$ at.%) with irradiation times of 30 s (**a**) and 5 min (**b**) and their corresponding *insets* show the variation of TL intensity as a function of Ce^{3+} ion concentration. **c–f** Show the variation nature of TL glow curves of $Na_3Sr_{1-x}B_5O_{10}:Ce_x^{3+}$ phosphors ($x = 0.5 - 5$ at.%) at 5 min of γ-ray irradiation time, respectively

It ranges from 0.7 to 0.9 and between 1.05 and 1.20 for first- and second-order kinetics, respectively. The calculated values are presented in Table 1, which is in good agreement with the geometrical factor values. Therefore, the activation energy (E) could be calculated using the following relation [33, 35]

$$E = C_\eta\left(kT_m^2/\eta\right) - b_\eta(2kT_m) \tag{7}$$

where η stands for τ, δ and ω, while $\tau = T_m - T_1$ and $\delta = T_2 - T_m$ are the low- and high-temperature half-widths, respectively, $\omega = T_2 - T_1$ is the full width and k is the Boltzmann's constant.

$$\begin{aligned} C_\tau &= 1.51 + 3\left(\mu_g - \Delta\right) \\ C_\delta &= 0.976 + 7.3\left(\mu_g - \Delta\right) \\ C_\omega &= 2.52 + 10.2\left(\mu_g - \Delta\right) \\ b_\tau &= 1.58 + 4.2\left(\mu_g - \Delta\right) \\ b_\delta &= 0 \\ b_\omega &= 1 \end{aligned} \tag{8}$$

Here, $\Delta = 0.42$ and 0.52 for first- and second-order TL peaks, respectively. Using the above equations, the activation energy (E) was estimated and is listed in Table 1. The value of frequency factor (s) can be obtained with the following equations,

$$\begin{aligned} \frac{\beta E}{kT_m^2} &= s\exp\left(\frac{-E}{kT_m}\right) \quad \text{and} \\ \frac{\beta E}{kT_m^2} &= s\exp\left(\frac{-E}{kT_m}\right)\left|1 + 2\frac{kT_m}{E}\right| \end{aligned} \tag{9}$$

for first- and second-order kinetics, respectively.where β is the heating rate (5 °C/s). The calculated values are summarized in Table 1. At 5-min irradiation time, the E and s values were 0.5998 eV and 2.75E07 s^{-1}, respectively, for 1 at.% Ce^{3+} ions.

4 Conclusion

In conclusion, a new $Na_3SrB_5O_{10}:Ce^{3+}$ blue-emitting phosphors were synthesized via a simple and facile high-temperature solid-state reaction route. The synthesized phosphors show triclinic structure upon calcination at 800 °C for 8 h. The $Na_3SrB_5O_{10}:Ce^{3+}$ phosphors exhibit intense single broad emission for all concentrations centered at about 370 nm under the 232 nm excitation. The energy transfer from Ce^{3+} to Ce^{3+} in $Na_3SrB_5O_{10}$

Table 1 Kinetic parameters from Chen's peak shape method in $Na_3SrB_5O_{10}:Ce^{3+}$ phosphors with γ-ray irradiation times of 30 s and 5 min, scanning rate of 5 °C/s at 0.58 Gyh^{-1} for 5 Gy

t	x (at.%)	T_1 (°C)	T_m (°C)	T_2 (°C)	τ (°C)	δ (°C)	ε (°C)	Shape factor		b	Activation energy E (eV)				Frequency factor s (s^{-1})			
								μ	γ		E_τ	E_δ	E_ε	E_{mean}	s_τ	s_δ	s_ε	s_{mean}
30 s	0.5	138.71	189.50	226.26	50.79	36.76	87.55	0.42	0.72	1	0.4219	0.4889	0.4505	0.4538	2.52E05	1.57E06	5.52E05	7.91E05
	1	148.19	194.30	228.68	46.11	34.38	80.49	0.43	0.74	1	0.4953	0.5627	0.5256	0.5278	1.61E06	9.74E06	3.62E06	4.99E06
	3	154.15	194.59	229.38	40.44	34.79	75.23	0.46	0.86	1	0.6211	0.6963	0.6589	0.6588	4.54E07	3.29E08	1.23E08	1.66E08
	5	111.75	153.82	202.35	42.07	48.53	90.6	0.53	1.15	2	0.4599	0.3526	0.3907	0.4011	1.89E06	7.54E04	2.39E05	7.36E05
5 min	0.5	147.49	201.56	241.61	54.07	40.05	94.12	0.42	0.74	1	0.4167	0.4924	0.4494	0.4528	1.59E05	1.20E06	3.82E05	5.80E05
	1	157.28	200.31	233.69	43.03	33.38	76.14	0.44	0.77	1	0.5654	0.6356	0.5985	0.5998	8.55E06	5.36E07	2.04E07	2.75E07
	3	175.00	218.33	259.63	43.33	41.3	84.63	0.49	0.95	2	0.5564	0.3739	0.4545	0.4616	3.29E06	3.16E04	2.35E05	1.19E06
	5																	
	Peak I	142.66	195.89	246.05	53.23	50.16	103.39	0.49	0.94	2	0.3843	0.2725	0.3158	0.4694	6.31E04	3.15E03	9.16E03	3.40E06
	Peak II	252.25	298.52	344.73	46.27	46.21	92.48	0.50	0.99	2	0.7342	0.5041	0.6053		1.91E07	1.26E05	1.12E06	

t = γ-ray irradiation time; x = dopant ion concentration in host; b = order of kinetics

phosphor was found to be the exchange interaction, and the critical distance (R_c) calculated by the concentration quenching is ~34.09 Å. The highest TL intensity peaking at high-temperature side about 200.31 °C was obtained for 1 at.% Ce^{3+} in the present host, due to the high-energy traps formed during irradiation. Because of the simple TL glow curve (200.31 °C), strong blue emission and well-defined microstructure make these promising materials potentially applied in thermoluminescence dosimetry.

Acknowledgments B. Deva Prasad Raju is thankful to the Department of Science and Technology of the Government of India for providing financial assistance in the form of a Major Research Project (Fast Track Research Project Young Scientist Award); vide reference no: DST-SR/FTP/PS-198/2012; dated: 14.02.2014. This work was partially supported by the New and Renewable Energy Core Technology Program of the Korea Institute of Energy Technology Evaluation and Planning (KETEP), granted financial resource from the Ministry of Trade, Industry and Energy, Republic of Korea (No. 2012T100201679).

References

1. P. Becker, Adv. Mater. **10**, 979 (1998)
2. X. Zhang, J. Song, C. Zhou, L. Zhou, M. Gong, J. Lumin. **149**, 69 (2014)
3. R. Yu, S. Zhong, N. Xue, H. Li, H. Ma, Dalton Trans. **43**, 10969 (2014)
4. L.H. Jiang, Y.L. Zhang, C.Y. Li, J.Q. Hao, Q. Su, Mater. Lett. **61**, 5107 (2007)
5. L.H. Jiang, Y.L. Zhang, C.Y. Li, R. Pang, J.Q. Hao, Q. Su, J. Lumin. **128**, 1904 (2008)
6. V. Dotsenko, J. Mater. Chem. **10**, 561 (2000)
7. G.C. Mishra, A.K. Upadhyay, S.K. Dwiwedi, S.J. Dhoble, R.S. Kher, J. Mater. Sci. **47**, 2752 (2012)
8. L.Y. Liu, Y.L. Zhang, J.Q. Hao, C.Y. Li, Q. Tang, C.X. Zhang, Q. Su, Mater. Lett. **60**, 639 (2006)
9. F. Yang, Y. Liang, M. Liu, X. Li, M. Zhang, N. Wang, Opt. Laser Technol. **46**, 14 (2013)
10. A. Kitai, *Luminescent Materials and Application* (Wiley, England, 2008)
11. L. Chen, Y. Gao, Mater. Chem. Phys. **116**, 242–246 (2009)
12. X.B. Qiao, Y. Cheng, C.X. Qin, Z.X. Tao, Y.L. Huang, P. Cai, C. Chen, H.J. Seo, Appl. Phys. A **118**, 749 (2015)
13. G. Blasse, B.C. Grabmaier, *Luminescent Materials* (Springer, Berlin, 1994)
14. J. Wen, L. Ning, C.K. Duan, Y. Chen, Y. Zhang, M. Yin, J. Phys. Chem. C **116**, 20513 (2012)
15. V.C. Kongre, S.C. Gedam, S.J. Dhoble, J. Lumin. **135**, 55 (2013)
16. Y. Wu, G. Ren, Cryst. Eng. Comm. **15**, 4153 (2013)
17. A.A. Setlur, W.J. Heward, M.E. Hannah, U. Happek, Chem. Mater. **20**, 6277 (2008)
18. X. Zhang, H. Lang, H.J. Seo, J. Fluoresc. **21**, 1111 (2011)
19. L. Wu, G. Roth, K. Sparta, X. Chen, Acta Cryst. C **64**, i53 (2008)
20. G.R. Dillip, S.J. Dhoble, B.D.P. Raju, Opt. Mater. **35**, 2261 (2013)
21. W.B. Im, N.N. Fellows, S.P. DenBaars, R. Seshadri, Y.I. Kim, Chem. Mater. **21**, 2957 (2009)
22. W.R. Liu, C.H. Huang, C.P. Wu, Y.C. Chiu, Y.T. Yeh, T.M. Chen, J. Mater. Chem. **21**, 6869 (2011)
23. X. Chen, M. Li, X. Chang, H. Zang, W. Xiao, J. Solid State Chem. **180**, 1658 (2007)

24. G.R. Dillip, K. Mallikarjuna, S.J. Dhoble, B.D.P. Raju, J. Phys. Chem. Solids **75**, 8 (2014)
25. J. Zhou, Z. Xia, M. Yang, K. Shen, J. Mater. Chem. **22**, 21935 (2012)
26. J. Chen, W. Zhao, J. Zhong, L. Lan, J. Wang, N. Wang, Ceram. Int. **40**, 15241 (2014)
27. Y. Zhang, G. Li, D. Geng, M. Shang, C. Peng, J. Lin, Inorg. Chem. **51**, 11655 (2012)
28. Y. Nagaoka, S. Adachi, J. Lumin. **145**, 797 (2014)
29. B.P. Kore, N.S. Dhoble, S.J. Dhoble, Radiat. Meas. **67**, 35 (2014)
30. D.L. Dexter, J. Chem. Phys. **21**, 836 (1953)
31. L.G.V. Uitert, J. Electrochem. Soc. **114**, 1048 (1967)
32. G. Blasse, J. Solid State Chem. **62**, 207 (1986)
33. R. Chen, J. Electrochem. Soc. **116**, 1254 (1969)
34. M. Balarin, J. Therm. Anal. **17**, 319 (1979)
35. J. Azorin, C. Furetta, A. Gutierrez, J. Phys. D Appl. Phys. **22**, 458 (1989)